

Dependence of tropical-cyclone intensification on the boundary layer representation in a numerical model

Roger K. Smith^a * and Gerald L. Thomsen^a

^a Meteorological Institute, University of Munich, Munich, Germany

Abstract:

We present idealized numerical model experiments to investigate the structure of the boundary layer in a tropical cyclone. The study is motivated by recent findings highlighting the important dynamical role of the boundary layer to tropical-cyclone intensification. The calculations are carried out using the Pennsylvania State University–National Center for Atmospheric Research fifth-generation Mesoscale Model (MM5). Predictions using one of five of the available schemes are compared, not only between themselves, but where possible with recent observational analyses of boundary layer structure. At this stage the study falls short of being able to advocate the use of a particular scheme, although certain shortcomings of individual schemes are identified. The current inability to determine “the optimum scheme” has implications for the predictability of tropical-cyclone intensification. Copyright © 2009 Royal Meteorological Society

KEY WORDS Hurricane; tropical cyclone; typhoon; boundary layer; vortex intensification

Received November 17, 2009; Revised ; Accepted

1 Introduction

In a recent paper, Smith *et al.* (2009; henceforth M3) revisited the problem of interpreting the dynamics of tropical cyclone intensification in a three-dimensional numerical model. They showed that, from an azimuthally-averaged viewpoint, there are two mechanisms for vortex intensification, both involving the radial convergence of absolute angular momentum, M . This quantity is related to the azimuthally-averaged tangential wind speed, v , by the formula: $v = M/r - \frac{1}{2}fr$, where r is the radius of an air parcel from the vortex centre and f is the Coriolis parameter. In the absence of friction, M is a materially-conserved quantity so that both terms in the above expression lead to an increase in v as r decreases, and conversely.

The first mechanism for intensification is associated with radial convergence of M above the boundary layer[†] in conjunction with its conservation. The convergence is produced by increasing system-scale[‡] radial buoyancy gradients associated with deep, inner-core convection in the presence of enhanced surface moisture fluxes. This mechanism has been articulated previously by many authors (e.g. Ooyama 1969, Willoughby 1988, 1995). It explains why the vortex expands in size and may

be interpreted in terms of balanced dynamics (Bui *et al.* 2009).

The second mechanism is associated with radial convergence of M within the boundary layer and becomes important in the inner-core. Although M is not materially conserved in the boundary layer, the largest wind speeds anywhere in the vortex can be achieved in or at the top of the boundary layer if the radial inflow is sufficiently large to bring the air parcels to small radii with a minimal loss of angular momentum (in other words the reduction of M in the formula for v is more than offset by the reduction in r). This mechanism explains why the maximum azimuthally-averaged tangential wind speeds in the model calculations of M3 and in those of other authors (e.g. Zhang *et al.* 2000) are located at low levels near the top of the boundary layer. Of course, the radial inflow in both mechanisms is ultimately linked to the ascent forced by the local buoyancy of individual deep convective clouds in the inner-core region (Montgomery *et al.* 2009), but the boundary-layer inflow is considerably enhanced by the force imbalance brought about by surface friction (Bui *et al.* 2009).

An alternative, but equivalent interpretation for the material acceleration of the mean tangential wind follows directly from Newton's second law in which the sole force is the generalized Coriolis force, $-u(v/r + f)$, where u is the mean radial velocity component. If the flow is convergent, $u < 0$, so that this force is positive and leads to an acceleration of v . If friction is present, but if rings of air converge quickly enough (i.e. if u is sufficiently large), the generalized Coriolis force can exceed the tangential component of frictional force and the tangential winds will increase with decreasing radius in the boundary layer as well. It is precisely for this reason that supergradient

*Correspondence to: Roger K. Smith, Meteorological Institute, University of Munich, Theresienstr. 37, 80333 Munich, Germany. Email: roger.smith@lmu.de

[†]As in M3 we use the term boundary layer to describe the shallow layer of strong inflow near the sea surface that is typically 500 m to 1 km deep and which arises largely because of the frictional disruption of gradient wind balance near the surface.

[‡]The concepts of system-scale and local buoyancy in rapidly-rotating vortices is discussed by Smith *et al.* (2005).

winds can arise in the boundary layer (see e.g. Nguyen *et al.* 2002, Smith and Vogl 2008).

The foregoing results indicate that the spin-up of the vortex core is tied fundamentally to the dynamics of the boundary layer, highlighting the central importance of the boundary layer and its representation in numerical models for the prediction of tropical-cyclone intensification. Most numerical weather prediction models employ a sophisticated parameterization scheme for the boundary layer and the question naturally arises: *what is the most appropriate scheme for the prediction of tropical cyclone intensification?*

An early study demonstrating the importance of resolving the boundary layer was that by Anthes and Chang (1978). They carried out simulations of hurricanes using a model with high vertical resolution in the boundary layer, with a relatively coarse resolution above this layer and with a coarse 60-km horizontal grid spacing. They compared the model with high resolution in the boundary layer (a nine-level model) to one treating the boundary layer as a single layer (a five-level model). They found that the extra resolution of the boundary layer affected the behaviour of the simulated storms and their sensitivity to changes in surface properties, although their structures above the boundary layer were similar. Their study raised questions about the sensitivity of more sophisticated, higher-resolution models to the parameterization of boundary layer processes and whether some boundary-layer schemes may be more predisposed toward developing strong hurricanes than others.

Motivated by the above question, Braun and Tao (2000) carried out high resolution simulations of Hurricane Bob (1991) using the Pennsylvania State University National Center for Atmospheric Research fifth-generation Mesoscale Model (MM5; Dudhia 1993; Grell *et al.* 1995). Tests were conducted to determine the sensitivity of the simulation to the available planetary boundary layer parameterizations in MM5, including the bulk aerodynamic, Blackadar, Medium-Range Forecast (MRF) model, and Burk Thompson boundary-layer schemes. Significant sensitivity was found between the calculations with minimum central pressures varying by up to 16 mb and maximum winds by 15 m s^{-1} , but all of the calculations overestimated the observed intensity of the storm. Simulated horizontal precipitation structures varied substantially between the different schemes, suggesting that accurate forecasts of precipitation in hurricanes can be just as sensitive to the formulation of the boundary layer representation as they are to the cloud microphysical parameterizations. At the time of their study, the boundary layer was thought of mainly as providing the moisture source to fuel the eyewall convection. However, following the findings of M3, it is seen as playing a direct dynamic role in the spinup process, a recognition that calls for a more comprehensive reappraisal of different boundary layer parameterizations with a particular focus on the processes articulated in M3.

BT00 chose to assess different boundary layer schemes in a single case study, presumably with a view

to identifying the most skillful scheme. However, it turned out that none of the schemes reproduced the intensification of Hurricane Bob especially well. A similar case study has been carried out recently by Nolan *et al.* (2009a,b), who examined two boundary-layer schemes in the Weather Research and Forecasting Model (WRF), the Yonsei University and the Mellor-Yamada-Janjic schemes. They examined also two modifications of these schemes. Their study focussed on the mature hurricane stage and the main conclusion seemed to be that although there were many differences in detail between the schemes, all the simulations were “... in good agreement with the detailed analyses of in-situ data ...”. Notably, the study fell short of recommending a particular scheme, although it did caution that a particular scheme might be sensitive to the model in which it used.

As a further step to compare different boundary-layer schemes in the tropical-cyclone context, we examine here the behaviour of five boundary-layer schemes available in MM5 in an idealized model configuration. This approach has the advantage that it avoids many of the complications inherent in studies of individual cases with full-physics models, but it has the disadvantage of making comparisons with observations a little less direct. The calculations are based on the thought experiment discussed by Nguyen *et al.* (2008; henceforth M1), which considers the spin-up of an initially-symmetric vortex on an f -plane in a quiescent environment. Where possible we compare the structure of the low-level winds with those of recent observational studies including those of Franklin *et al.* (2003), Kepert (2006a,b) and Bell and Montgomery (2008). While these comparisons fall short of enabling us to determine “the optimum scheme” for reasons discussed later, they do allow us to determine the range of variation between different schemes in the light of recent findings concerning the dynamics of the boundary layer (Smith 2003, Smith and Vogl 2008, M3). Moreover, the calculations have implications for the predictability of tropical cyclone intensity.

The paper is organized as follows. The numerical experiments are described in section 2, including the derivation of initial conditions and modifications to some of the model physics. Section 3 provides a brief description of boundary layer schemes, with more details given in an appendix. The results are described in sections 4 and the conclusions are given in section 5.

2 The model configuration

The numerical experiments are similar to those described in M1. They are carried out using a modified version of MM5 (version 3.6) (Dudhia 1993; Grell *et al.* 1995). The model is configured with three domains: a coarse mesh of 45-km resolution and two, two-way nested domains of 15 and 5 km resolution, respectively. The domains are square and are 9000 km, 4500 km, 1500 km on each side. The calculations are performed on an f -plane centred at 20°N . In all calculations there are 24 σ -levels in the vertical, 10 of which are below 850 mb. The model top is at a pressure

No.	Scheme	Brief description
1	Bulk	Surface fluxes of sensible heat, latent heat and momentum determined by a bulk-aerodynamic formula. Fluxes within the boundary layer calculated by a first-order (local K -mixing) scheme.
2	Blackadar	Vertical transfer of momentum, heat and moisture is determined by (non-local) transilient mixing. The surface layer fluxes are based on Monin-Obukhov similarity theory.
3	Burk-Thompson	M-Y level 2.5 with TKE prediction. The eddy exchange coefficient of an adiabatically conserved quantity is related to the predicted turbulent kinetic energy (TKE). The Louis (1979) scheme is used to parameterize the surface layer.
4	MRF	Local k -mixing with counter-gradient correction of q and θ . The surface layer fluxes are based on Monin-Obukhov similarity theory.
5	Gayno-Seaman	M-Y level 2.5 with TKE prediction, including horizontal and vertical advection and horizontal diffusion of TKE. The eddy exchange coefficient of an adiabatically conserved quantity is related to the predicted turbulent kinetic energy (TKE). A countergradient correction for θ_l (liquid-water potential temperature) is applied. Surface layer fluxes are based on Monin-Obukhov similarity theory.

Table I. Boundary-layer schemes used in this study with a brief description of each scheme. Versions of the Bulk scheme and Gayno-Seaman scheme with their default values for the exchange coefficients are studied also.

level of 50 mb. The precise σ -levels are: $\sigma = 1.00, 0.995, 0.990, 0.980, 0.970, 0.960, 0.950, 0.930, 0.910, 0.890, 0.850, 0.810, 0.770, 0.730, 0.690, 0.650, 0.610, 0.570, 0.530, 0.490, 0.450, 0.300, 0.150$ and 0.00 .

In order to keep the experiments as simple as possible, we choose the simplest explicit moisture scheme, one that mimics pseudo-adiabatic ascent as discussed in M1. In addition we choose one of five boundary-layer schemes available in the model as detailed in subsection 2.1. The moisture and boundary-layer schemes are applied in all domains. The sea surface temperature is set to a constant 27°C . For simplicity, radiative cooling is neglected. The initial vortex is axisymmetric with a maximum tangential wind speed of 15 m s^{-1} at the surface at a radius of 135 km. The strength of the tangential wind decreases sinusoidally with height, vanishing at the top model level (50 mb). The temperature field is initialised to be in gradient wind balance with the wind field using the method described by Smith (2006). The far-field temperature and humidity are based on Jordan's Caribbean sounding (Jordan 1958). The vortex centre is defined as the centroid of relative vorticity at 900 mb over a circular region of 200 km radius from a "first-guess" centre, which is determined by the minimum of the total wind speed at 900 mb.

2.1 The boundary-layer schemes

The five boundary-layer schemes examined here are listed in Table I together with a brief description of each. Further details are given in an appendix. In the main series of calculations, the surface drag and heat and moisture exchange coefficients are modified in all of the schemes to facilitate a proper comparison. These coefficients are chosen to fit the results of the coupled boundary layer air-sea transfer experiment (CBLAST), described by Black *et al.* (2007). The moisture exchange coefficient, C_E , is

set to 1.2×10^{-3} and the drag coefficient, C_D , is set to $0.7 \times 10^{-3} + 1.5 \times 10^{-3} \exp(0.05|\mathbf{u}|)$, where $|\mathbf{u}|$ is the wind speed at the lowest model level. Two additional calculations are described briefly in which the Bulk scheme and Gayno-Seaman scheme are used with the default values for their surface exchange coefficients to assess the impact of changing these coefficients. These default values are detailed in the appendix also.

3 Results

3.1 Time evolution

Figure 1 shows time-series of the maximum azimuthally-averaged radial and tangential wind components, and the maximum azimuthally-averaged radial inflow component in the lowest 3 km in the set of seven calculations with different boundary layer parameterizations (labelled 1-5), including those with the Bulk- and Gayno-Seaman schemes with their default surface exchange coefficients (labelled 6 and 7, respectively). As judged by the maximum azimuthally-averaged tangential wind speed[§], the earliest onset of rapid intensification occurs in the modified Bulk scheme (Figure 1a) and the Gayno-Seaman scheme with its default surface exchange coefficients (Figure 1b). Rapid intensification in the other calculations occurs 6-12 hours later, except in the MRF scheme where

[§]M1 noted that deep convective cores containing enhanced low-level rotation were the coherent structures of the intensification process and that the details of these structures are sensitive to the low-level moisture distribution. They carried out a series of ensemble calculations to examine the sensitivity of the control calculation to small randomly-distributed perturbations of the initial moisture in the lowest 100 mb and found a spread in the calculated intensity between ensemble members at any given time. This spread had a standard deviation on the order of $\pm 7 \text{ m s}^{-1}$ during the period of rapid intensification and a little less in the mature stage at 96 hours. They concluded that any differences in intensity less than this amount between two deterministic calculations were not significant.

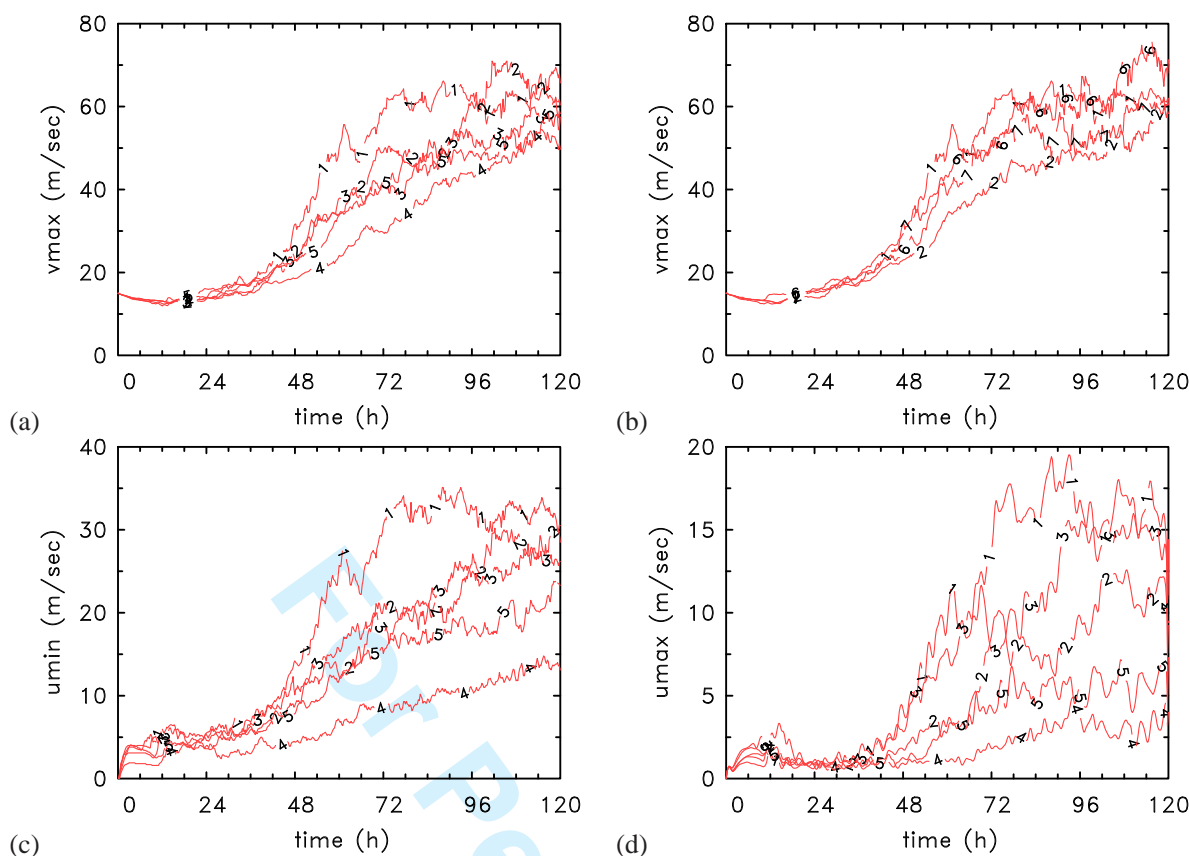


Figure 1. Time-series of (a), (b) maximum azimuthally-averaged tangential wind speed, (c) minimum azimuthally-averaged radial wind speed, and (d) maximum azimuthally-averaged radial wind speed in the lowest 3 km in the set of calculations with different boundary layer parameterizations: 1 = Bulk scheme, 2 = Blackadar scheme, 3 = Burk-Thompson scheme, 4 = MRF scheme, 5 = Gayno-Seaman scheme, 6 = Bulk scheme with default exchange coefficients, 7 = Gayno-Seaman scheme with default exchange coefficients. Note the different scales on the ordinate of each panel.

the intensification rate is the most sluggish. With this scheme, the vortex takes more than a day longer to reach hurricane strength (33 m s^{-1}) than with the Bulk scheme. The Bulk scheme with the default exchange coefficients (curve 6 in Figure 1b) gives the largest intensity after 5 days of almost 70 m s^{-1} , while the intensities of the other schemes range between 50 m s^{-1} and 60 m s^{-1} . The differences between the pair of calculations with the Bulk scheme and the pair with the Gayno-Seaman scheme are probably only marginally significant in the light of the findings of M1. The differences between the intensity after 5 days between the seven calculations is about 20 m s^{-1} , this intensity being highest with the Blackadar scheme and lowest with the MRF scheme.

The foregoing results are a little different from those of BT00, who found that the Burk-Thompson schemes and Bulk produced the strongest storm, but they found also that the MRF scheme produced the weakest one. The differences between schemes are comparable with those reported by BT00, who found differences reaching up to 22 m s^{-1} during their 72 hour integration. It is pertinent to note, however, that in the main comparisons of schemes described in their section 4, the schemes in BT00 had different surface exchange coefficients.

The maximum inflow and outflow show considerable differences also between the five schemes (panels (c) and

(d) of Figure 1). These quantities were not shown by BT00, but following the work of M3 are considered to be important. During the period of rapid intensification, the largest inflow occurs with the modified Bulk scheme, with the speed reaching 35 m s^{-1} between 90 and 96 hours, before decreasing a little. By far the weakest inflow occurs in the MRF scheme with the speed not quite reaching 15 m s^{-1} . The three other schemes including the modified Bulk and Gayno-Seaman schemes have maximum radial inflow speeds after 5 days lying in the range $24\text{--}30 \text{ m s}^{-1}$. In broad terms, the inflow velocity is important as it determines how close to the rotation axis air parcels can penetrate in the boundary layer, which, in turn, determines how fast they may spin, even though they lose a fraction of their absolute angular momentum as a result of friction as discussed in Smith *et al.* (2008) and in M3. An alternative view is that, since the advective contribution to the total tangential wind tendency is dominated by the radial advection of absolute vorticity, the spin-up rate is intimately coupled with the radial wind speed component (see e.g. Bui *et al.* 2009). The maximum outflow shown in panel (c) is discussed below. Panel (d) of Figure 1 is discussed in the next section.

3.2 Mature stage wind structure

The differences in the wind structure between the five schemes (including the two versions of the Bulk scheme) are highlighted by the radius-height cross-sections of azimuthally-averaged radial and tangential wind components in the lowest 3 km, averaged between 108 and 120 hours of integration, when the vortex has reached its mature stage. These cross-sections are shown in Figure 2 and the extreme values of these quantities and their locations are summarized in Table II. A common feature of all six calculations is the shallow region of inflow that characterizes the boundary layer and a region of outflow that surmounts it at small radii. With the MRF and Gayno-Seaman schemes (panels (e) and (f)), the inflow is weaker than in the other schemes and much weaker with the MRF scheme. The outflow maximum with the MRF scheme is not evident with the chosen contour interval and it is barely evident in the Gayno-Seaman scheme. In all cases, the maximum tangential wind component occurs close to the top of the inflow layer. This feature was discussed in M3. Note, however, there are appreciable differences in the structure of both velocity components between different schemes. In particular, the depth and strength of the low-level inflow vary between the schemes, as does the radius at which the maximum inflow occurs (see Table II). With the unmodified Bulk scheme and the MRF scheme, the maximum inflow occurs at the surface, whereas in the other schemes it is slightly elevated, between 100 and 200 m.

The forgoing structural differences are similar to those obtained by BT00, except that they found that the Burk-Thompson scheme gave the strongest vortex with the maximum inflow, while the Bulk scheme was marginally weaker in both respects (see their Figures 9 and 10). BT00 showed fields throughout the whole troposphere, whereas we focus attention here on the lower troposphere below a height of 3 km. BT00 found also that the MRF scheme gives the deepest and weakest inflow, the weakest tangential wind maximum, and that it is the only scheme not to show a low-level outflow maximum at the contour level plotted, as in our study. It is interesting to note that the depth of the strong inflow layer, as judged by the $u = -5 \text{ m s}^{-1}$ contour, increases inwards in all cases until a radius ranging from about 85 km with the MRF scheme to about 55 km with the unmodified Bulk scheme. Thereafter the depth decreases as the radial flow declines towards the rotation axis.

The strength, radius and height of the maximum radial outflow varies also. Time-series of the maximum strength of the radial outflow below 3 km are shown in panel (d) of Fig. 1. These time-series exhibit considerable variability and have been smoothed by applying a 1-2-1 filter four times. They show that the outflow in the MRF scheme is weakest at all times with maximum values of only a few m s^{-1} and it is strongest with the modified Bulk scheme and Burk-Thompson scheme, with maximum values in the range 15-20 m s^{-1} after 3 to 4 days. Again, these results are broadly in line with those of BT00 (see their Figures 9 and 10).

3.3 Comparison with observations

Panels (g), (h) and (i) of Figure 2 show for comparison radius-height cross-sections of azimuthally-averaged radial and tangential wind components in the lowest 3 km obtained from analyses of data collected in Hurricane Isabel (2003) (Bell and Montgomery, 2008). These data were obtained on three days (12-14 September) when Isabel was a Category 5 storm and therefore stronger than the vortices in panels (a)-(f). While there are significant differences in detail between the observations, they do show a common feature between themselves and with our calculations, namely that the maximum tangential wind lies within the inflow layer or just on its boundary as predicted in M3. Moreover, the inflow is surmounted by a layer of radial outflow. One striking feature of the observations on 13 September not seen on other days nor in any of the calculations is that the maximum tangential wind lies well within the inflow layer. At this stage we are unable to offer an explanation for this feature.

3.4 Mature stage total wind structure

Hurricane forecasters are interested especially in the pattern of total wind speed and in particular how the near-surface wind speed is related to that determined from aircraft reconnaissance flights, which normally fly at a pressure altitude of 700 mb, equivalent to a height of about 2.9 km. For this reason we show in Figure 3 the isotachs of total wind corresponding with the wind components in Figure 2. The details of the maxima and their location are summarized also in Table II. The total wind has an elevated maximum (V_{tmax}) in all schemes and its strength, time-averaged over the period 108-120 hours, varies between 51 m s^{-1} with the MRF scheme and 71 m s^{-1} for the unmodified Bulk scheme. The radius at which the maximum occurs ranges between 30 km for the modified Bulk scheme and 60 km for the MRF scheme and the height at which it occurs ranges between 0.5 km for the unmodified Bulk scheme and 1.2 km for the MRF scheme. It is seen in Figure 3 that a local low-level wind speed maximum occurs at all radii, except within a few tens of kilometres of the centre, depending on the scheme.

Panels (g), (h) and (i) of Fig. 3 show similar radius-height cross-sections obtained from the Hurricane Isabel analyses. As in Figure 2, the comparison is limited by the difference in intensity, both between the observations, themselves, on different days, and the calculations. Nevertheless the observations and calculations are qualitatively similar and the observations show also an elevated maximum of total wind.

3.5 Comparison with dropwindsondings

It is pertinent to compare vertical profiles of the total wind speed with those obtained by Franklin *et al.* (2003) from an analysis of GPS[†] dropwindsonde soundings in the inner core region of hurricanes. These authors constructed

[†]Global Positioning System.

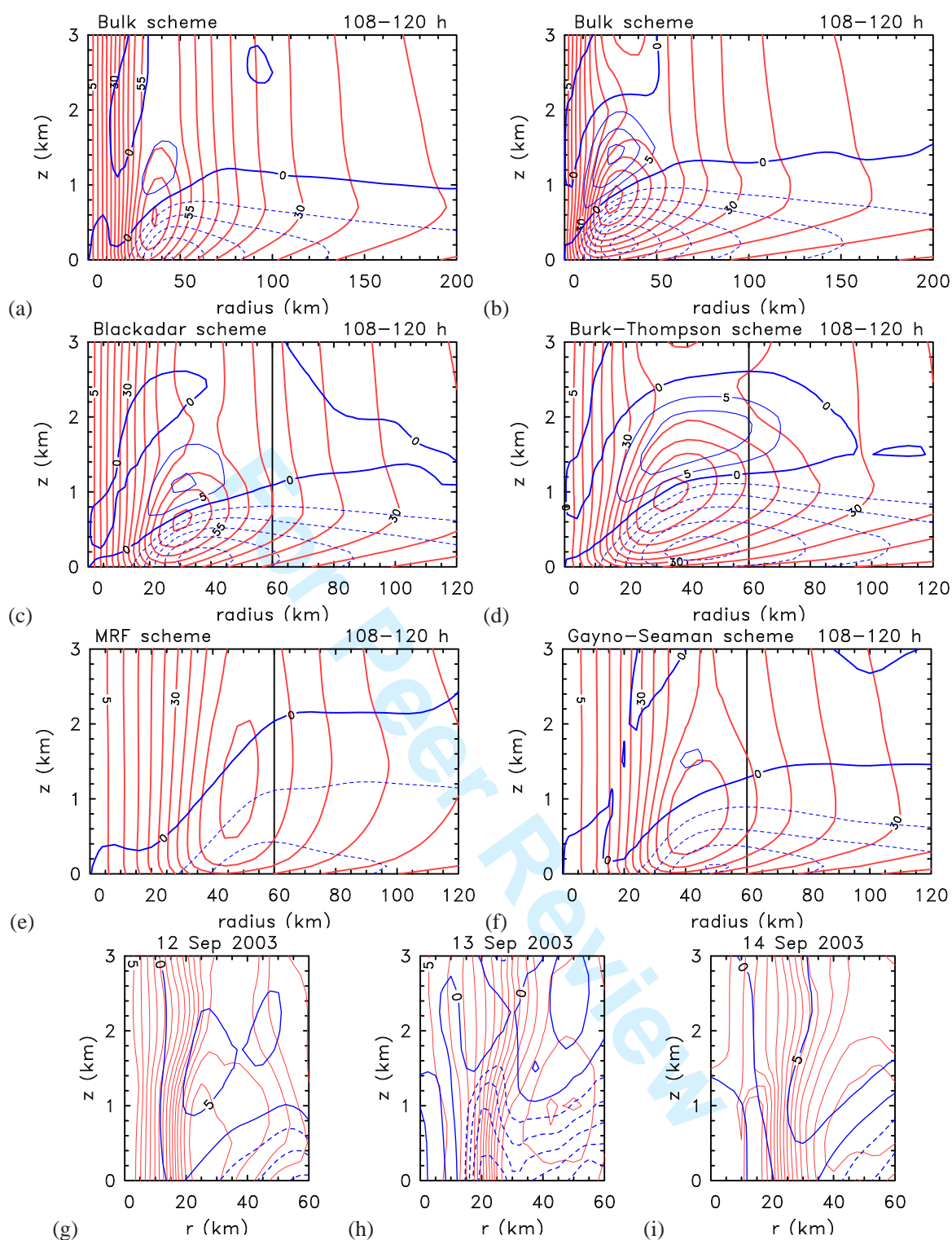


Figure 2. Radius-height cross-sections of azimuthally-averaged radial and tangential wind speed components in the lowest 3 km averaged at 15 minute intervals during the period 108–120 hours for the different boundary layer schemes. (a) unmodified Bulk scheme, (b) modified Bulk scheme, (c) Blackadar scheme, (d) Burk-Thompson scheme, (e) MRF scheme, and (f) Gayno-Seaman scheme. Contour interval 5 m s^{-1} . The zero contour is not plotted. Panels (g), (h) and (i) show similar cross-sections from analyses of data obtained on three days in Hurricane Isabel (2003) by Bell and Montgomery (2008). The solid vertical lines at 60 km radius in (a)–(f) delineate the region to compare with panels (g)–(i).

mean wind speed profiles for eyewall dropsondes released within 5.6 km (3 n mi) of the flight-level radius of maximum wind (RMW), for eyewall sondes released at least 7.4 km (4 n mi) radially outward of the RMW,

and for eyewall sondes released at least 7.4 km (4 n mi) radially inward of the RMW (their Fig. 10). Their data provide a useful benchline check of the boundary-layer schemes examined here. Figure 4 shows a comparison

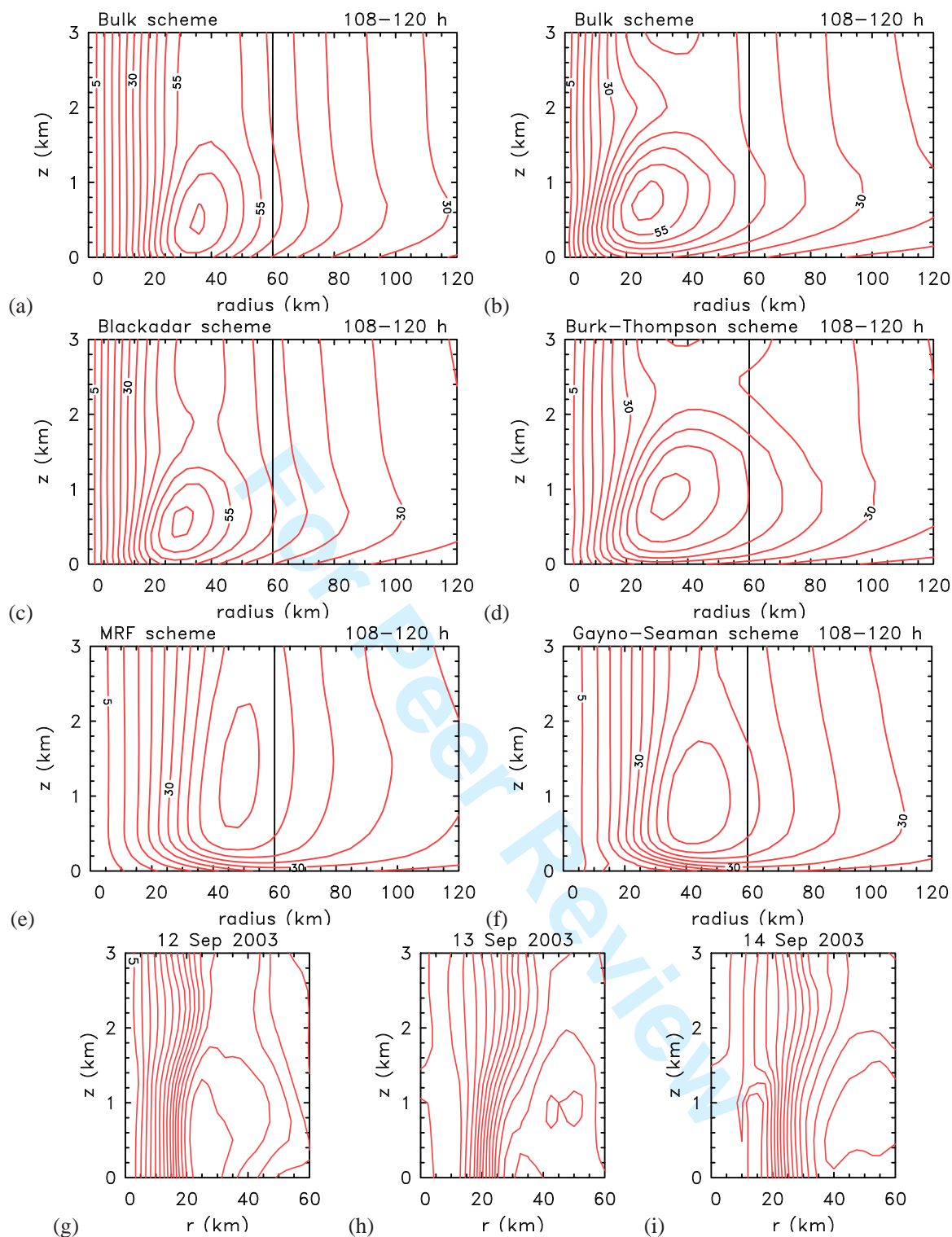


Figure 3. Radius-height cross-sections of azimuthally-averaged total wind speed in the lowest 3 km averaged at 15 minute intervals during the period 108–120 hours for the different boundary layer schemes. (a) unmodified Bulk scheme, (b) modified Bulk scheme, (c) Blackadar scheme, (d) Burk–Thompson scheme, (e) MRF scheme, and (f) Gayno–Seaman scheme. Contour interval 5 m s^{-1} . Panels (g), (h) and (i) show similar cross-sections from analyses of data obtained on three days in Hurricane Isabel (2003) by Bell and Montgomery (2008). The solid vertical lines at 60 km radius in (a)–(f) delineate the region to compare with panels (g)–(i).

of data derived from the five boundary-layer schemes compared with the data given in Franklin *et al.*'s Fig. 10. We examine similar vertical profile taken also at the radius of maximum total wind speed at a height of 2.9 km . It is seen that the MRF curve comes closest to reproducing

Franklin's RMW curve (labelled F1 in Figure 4), while the Gayno–Seaman curve lies close to Franklin's F2 curve. The F2 curve refers to the sondes released outside of the flight-level RMW and F3 to those released inside. The Burk–Thompson curve is the outlier, having a maximum

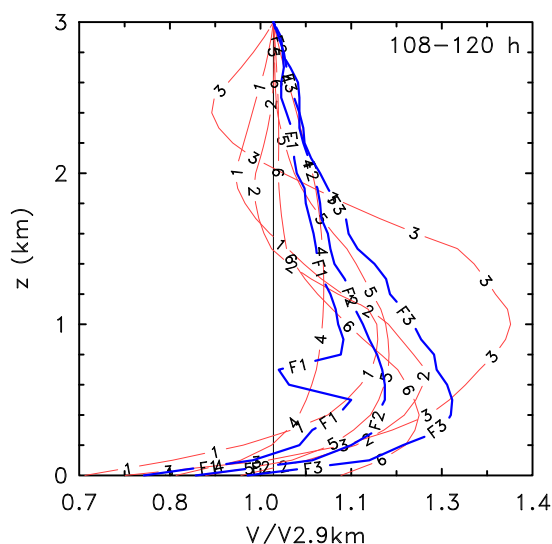
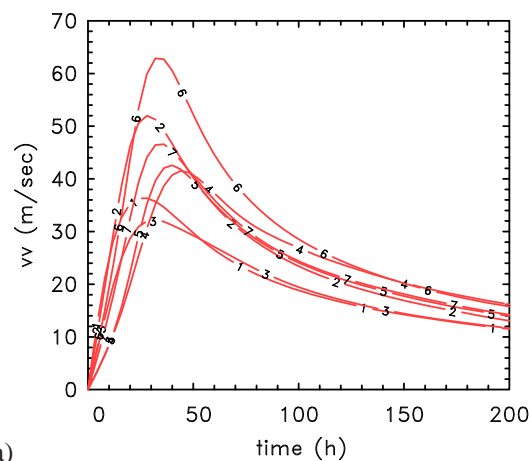


Figure 4. Vertical profiles of the ratio of azimuthal-mean total wind speed to that at 2.9 km at the radius of maximum tangential wind in the time-averaged fields from 108–120 h in the set of calculations with different boundary layer parameterizations: 1 = Bulk scheme, 2 = Blackadar scheme, 3 = Burk-Thompson scheme, 4 = MRF scheme, 5 = Gayno-Seaman scheme, 6 = unmodified Bulk scheme. The three thick curves show the mean wind speed profiles for eyewall dropsondes released within 5.6 km (3 n mi) of the flight-level RMW (labelled F1), for eyewall sondes released at least 7.4 km (4 n mi) radially outward of the RMW (labelled F2), and for eyewall sondes released at least 7.4 km (4 n mi) radially inward of the RMW (labelled F1) taken from Franklin *et al.* (2003). The sounding data are expressed as a percentage of the profile 700 mb wind speed, about 2.9 km in height.

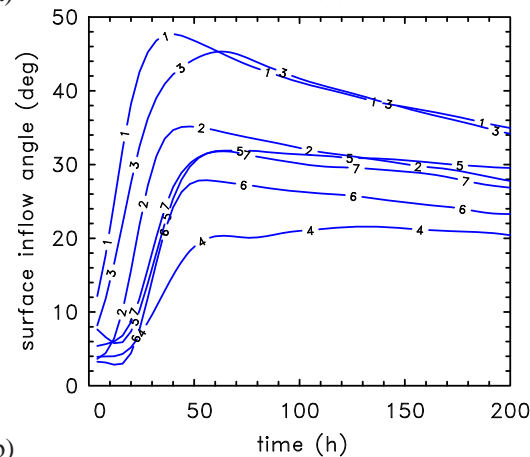
in excess of Franklin's F3 curve between 500 m and 1800 m and having the smallest values above about 2 km. The other schemes (the modified and unmodified Bulk schemes and the Blackadar scheme) are within the observed range of variability below 1–1.5 km, but are generally smaller than the observed curves above 1.5 km. The unmodified Bulk scheme has values that are too large compared with the observed curves near the surface. All except the unmodified Bulk scheme have maxima that are somewhat higher than those in the observations. Nevertheless, most of the schemes have a maximum ratio that is comparable in magnitude with those observed. In all schemes except the unmodified Bulk scheme, the ratio of near surface winds to winds at 2.9 km lie within the range found in the observations. In making these comparisons, it should be kept in mind that there is a lot of variability in the observational data from which the mean profiles are constructed.

3.6 Surface wind

Perhaps the feature of most immediate interest to hurricane forecasters from an axisymmetric perspective would be the radial profile of near-surface wind. Figure 6 shows radial profiles of azimuthal-mean total surface wind speed averaged during the period 108–120 hours in the five calculations together with the corresponding profiles of inflow angle ($\tan^{-1}(u/v)$), where u and v are the radial



(a)



(b)

Figure 5. (a) Radial profiles of azimuthal-mean total surface wind speed for the period 108–120 hours in the six calculations: 1 = Bulk scheme, 2 = Blackadar scheme, 3 = Burk Thompson scheme, 4 = MRF scheme, 5 = Gayno-Seaman scheme, 6 = unmodified Bulk scheme. (b) Corresponding inflow angles $\tan^{-1}(u/v)$.

and tangential velocity components. The strongest vortex at this time as measured by the surface wind is that with the unmodified Bulk scheme and the weakest is that with the Burk-Thompson scheme. The radius at which the maximum wind speed occurs varies from 27 km for the unmodified Bulk scheme to 47 km for the MRF scheme. As might be anticipated from Fig. 1, the inflow angles for the bulk scheme are rather large, the maximum of nearly 50° occurring at a radius of 40 km. The next largest angle is for the Burk-Thompson scheme, being about 45° at a radius of 65 km. Three other schemes have maxima in the range 20 – 35° and the MRF scheme has the smallest angle of about 20° . Surface inflow angles derived from recent observational studies of Hurricane Georges (1998), Hurricane Mitch (1998), Hurricane Danielle (1998) and Hurricane Isabel (2003) show maximum inflow angles of 24 deg., 18 deg., 24 deg., and 26 deg., respectively^{||}. From these data it must be concluded that the modified

^{||}The first of these angles is based on the right panels of the first and third rows of Figure 9 in Kepert (2006a); the second on panels (b) and (d) of Fig. 6 in Kepert (2006b); the third from the second panels of each column of Fig. 4 in Schwendike and Kepert (2008); and the fourth on the two right panels of Fig. 19 in the latter paper.

Scheme	unmod Bulk	mod Bulk	Blackadar	Burk-Thompson	MRF	Gayno-Seaman
vmax (m s ⁻¹)	70.5	61.4	66.0	56.6	51.4	54.3
rvmax (km)	36	24	32	36	48	40
zvmax (km)	0.6	0.7	0.7	1.0	1.1	0.7
umin (m s ⁻¹)	25.4	32.0	28.0	26.6	13.3	20.3
rumin (km)	44	32	36	40	52	48
zumin	0.0	0.2	0.1	0.2	0.0	0.1
umax (m s ⁻¹)	7.5	16.0	11.1	14.4	2.6	5.3
rumax (km)	36	28	32	44	48	40
zumax (km)	0.6	1.5	1.1	1.0	2.4	1.5
Vtmax (m s ⁻¹)	70.8	61.9	66.1	56.7	51.5	54.5
rVtmax (km)	45	30	40	45	60	55
zVtmax (km)	0.5	0.7	0.6	1.0	1.2	0.9

Table II. Maximum azimuthally-averaged tangential wind component (vmax), maximum and minimum azimuthally-averaged radial wind component (umax, umin), and maximum azimuthally-averaged total wind speed (Vtmax) averaged during the period 108-120 hours together with the radii (rvmax, rumax, rumin, rVtmax) and heights (zvmax, zumax, zumin, zVtmax) at which they occur for the five boundary-layer schemes, including the modified and unmodified versions of the Bulk scheme, as indicated.

Bulk and Burk-Thompson scheme considerably overestimate the surface inflow angle, while the other schemes give maximum inflow angles within, or a little above, the observed range of variation.

A relationship that is also of interest to hurricane forecasters is that between the maximum surface wind speed (V_{tsmax}) and the maximum wind speed (V_{tfmax}) at the flight level of typical reconnaissance aircraft (about 3 km) (Powell *et al.* 2009). In their observational study, Powell *et al.* found the typical ratio of these two wind maxima to be 0.83 with a standard deviation of 9%. The corresponding values for the six calculations in Figure 5 range from 0.7 for the Bulk scheme to 1.07 for the unmodified Bulk scheme. The average of all schemes is 0.90 with a standard deviation of 0.05. In all calculations, the radius of V_{tsmax} lies between 6-8 km *inside* that of V_{tfmax} , a value similar to that found by Powell *et al.*

3.7 Mature stage vertical velocity

Figure 6 shows radius-height cross-sections of azimuthal-mean vertical velocity averaged at 15 minute intervals for the 12-hour period 108-120 hours. All schemes have two local maxima, one at a height on the order of one to two kilometres and a second at a height of between 8 and 10 km as discussed in M3, although the lower maximum with the unmodified Bulk scheme is not apparent with the contour interval chosen in the figure and it does not exist with the MRF scheme. The strength and location of these maxima are summarized in Table III. Like the other fields, there are considerable differences in the strength of the maxima and the radii and heights at which they occur between the different schemes. The lower maximum ranges in strength between 1.0 m s⁻¹ and 2.0 m s⁻¹, its radius ranges between 20 and 36 km, and its height ranges between 0.8 km and 1.1 km. The upper maximum ranges in strength between 1.3 and 2.0 m s⁻¹, its radius ranges between 36 and 56 km, and its height ranges

between 8.1 km and 9.6 km. Again these differences are broadly similar to those found by BT00 as can be seen by comparing panels (a), (b), (c) and (e) of Figure 7 with panels (b), (c), (a) and (d), respectively, of BT00 Figure 8. In their case the maximum vertical velocities range from 0.75+ m s⁻¹ in the MRF scheme to 1.35+ m s⁻¹ in the Burk-Thompson scheme (these data are estimated from their contour plots and the values slightly exceed the highest contour: hence the '+' sign).

3.8 Mature stage agradient winds

An important feature of the boundary layer is the net inward force that develops at low levels outside the eyewall region as a result of friction. There the tangential flow is subgradient and the net force drives the strong inflow that is now recognized as being important for the spin-up of the inner core as discussed in M3. The net radial force, $-(1/\rho)(\partial p/\partial r) + v^2/r + fv$ is related to the agradient wind, v_a , defined at the azimuthal-mean tangential wind minus the gradient wind, v_g , defined by the positive solution of the gradient wind equation $v_g^2/r + fv_g - (1/\rho)(\partial p/\partial r) = 0$. Because of the importance of the agradient flow in the inner-core region, we show in Figure 8 radius-height cross-sections of v_a averaged at 15 minute intervals for the 12-hour period 108-120 hours. This quantity shows regions in which the flow deviates from gradient wind balance. Again there are considerable differences between the different schemes that are consistent with other features such as the strength of the inflow maximum and that of the low-level outflow maximum that overlies the inflow inside the eyewall.

The weakest pattern of agradient flow occurs in the MRF while the other three schemes show considerable departures from gradient flow in the inner core region, similar to that shown in Figure 6 of M3, which was based on the unmodified Bulk scheme. The largest magnitude of positive v_a in the six calculations ranges between 5.9 m

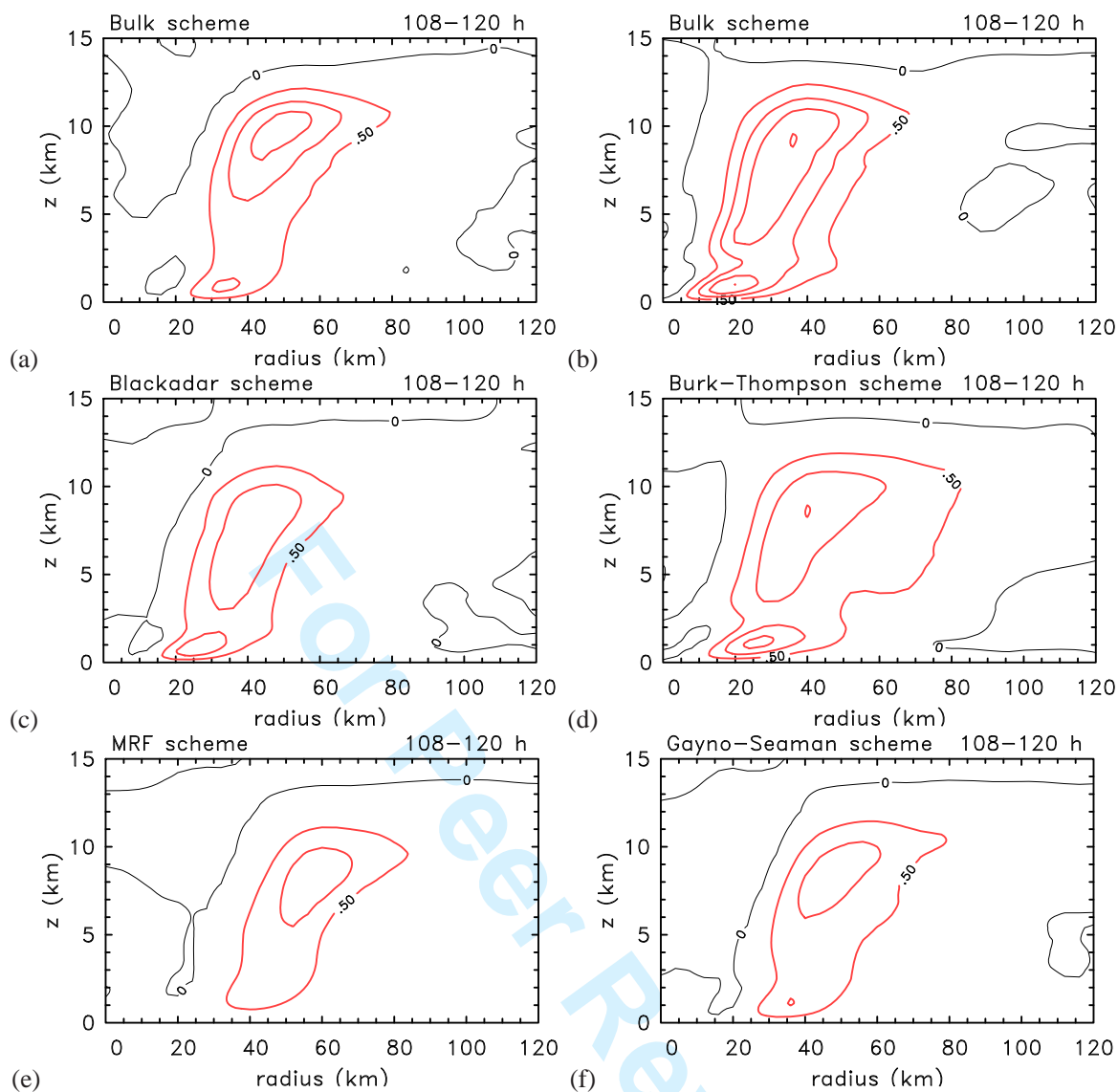


Figure 6. Radius-height cross-sections of azimuthally-averaged vertical velocity averaged at 15 minute intervals during the period 108-120 hours for the different boundary layer schemes. (a) unmodified Bulk scheme, (b) modified Bulk scheme, (c) Blackadar scheme, (d) Burk-Thompson scheme, (e) MRF scheme, and (f) Gayno-Seaman scheme. Contour interval 0.5 m s^{-1} . Thin black contours are zero contours. Note that, the isolated maximum below 2.5 km indicated in Table II for the MRF scheme is not evident in panel (e) with the chosen contour interval.

Scheme	unmod Bulk	mod Bulk	Blackadar	Burk-Thompson	MRF	Gayno-Seaman
wLmax (m s^{-1})	1.1	2.0	1.4	1.6	–	1.0
rwLmax (km)	32	20	28	24	–	36
zwLmax (km)	0.8	1.0	1.0	1.0	–	1.1
wUmax (m s^{-1})	1.7	2.0	1.5	1.5	1.4	1.3
rwUmax (km)	48	36	44	40	56	48
zwUmax (km)	9.6	9.2	8.4	8.6	8.1	8.5

Table III. Maximum vertical velocity (wLmax, wUmax) averaged during the period 108-120 hours together with the radii (rwLmax, rwUmax) and heights (zwLmax, zwUmax) at which they occur for the five boundary-layer schemes as indicated. Here “L” and “U” refer to isolated maximum vertical velocities below and above a height of 2.5 km, respectively.

s^{-1} for the MRF scheme and 17.4 m s^{-1} for the Burk-Thompson scheme. The average value for all six schemes is 13.9 m s^{-1} with a standard deviation of 1.5 m s^{-1} . This is a little higher than the observed values found by

Schwendike and Kepert (2008), which are on the order of 10 m s^{-1} , or about 12% of the gradient wind at 600 m. The radius of the maximum v_a is 24 km in all except the MRF and Gayno-Seaman schemes, where it is 32 km.

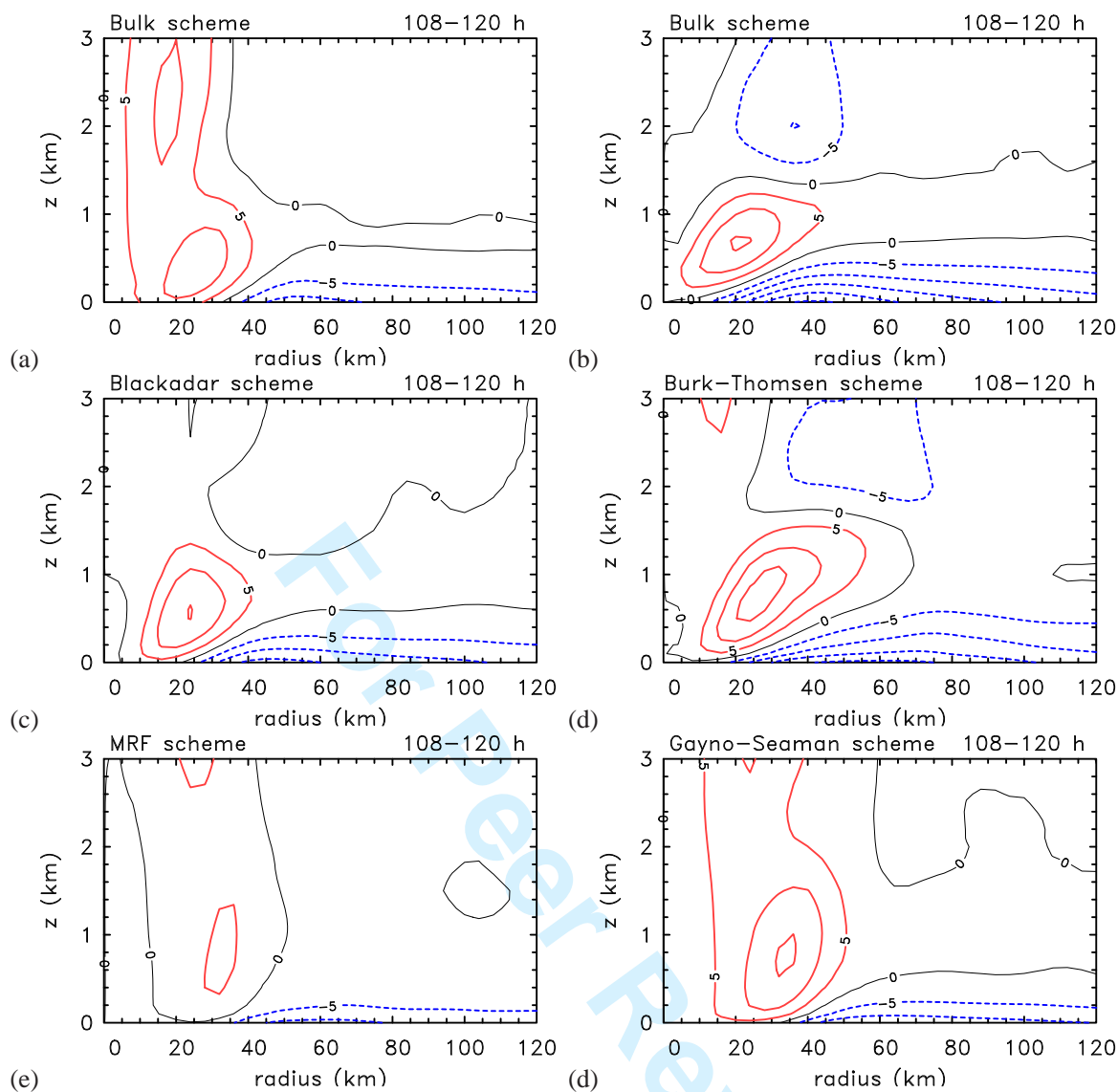


Figure 7. Radius-height cross-sections of azimuthally-averaged agradient wind during the period 108-120 hours for the different boundary layer schemes. (a) unmodified Bulk scheme, (b) modified Bulk scheme, (c) Blackadar scheme, (d) Burk-Thompson scheme, (d) MRF scheme, and (f) Gayno-Seaman scheme. Contour interval 5.0 m s^{-1} . Thin black contours are zero contours, dashed contours indicate negative values.

The height of the maximum v_a is 400 m in the unmodified Bulk scheme, 600 m in the Blackadar scheme and 700 m in all other schemes.

The largest magnitude of negative v_a ranges between 11.6 m s^{-1} for the MRF scheme and 25.7 m s^{-1} for the modified Bulk scheme. The average value for all six schemes is 17.0 m s^{-1} with a standard deviation of 2.1 m s^{-1} . The average radius of the minimum v_a is 53 km with a standard deviation of 3.3 km and the height of the minimum occurs at the surface in all schemes.

3.9 Mature stage thermodynamic structures

In view of their relevance to the global storm energetics as explained in a series of papers by Emanuel (see Emanuel 2004 for a recent review and a list of references), BT00 examined the structure of the thermodynamic fields as determined by the various schemes. For the same reason

we show in Figure 8 radial profiles of azimuthal-mean surface latent and sensible heat fluxes for the period 108-120 hours in the five calculations and in Figure 9 the corresponding profiles of pseudo-equivalent potential temperature for this period. As expected from many other studies (e.g. Smith and Vogl 2008), the latent heat fluxes are appreciably larger than the sensible heat fluxes. Notably, the surface heat fluxes are not all of the same sign, indicating that in some schemes, the near-surface air temperature slightly exceeds the sea-surface temperature.

There is a marked difference in the radial gradient of θ_e between the surface and 1.5 km. The near surface values carry a strong imprint of the radial distribution of the surface latent heat flux whereas that at 1.5 km is modified significantly by advection and vertical diffusion and has a larger radial gradient than that at the surface. As argued by Emanuel (1986), the radial gradient above the boundary layer determines to a first approximation the

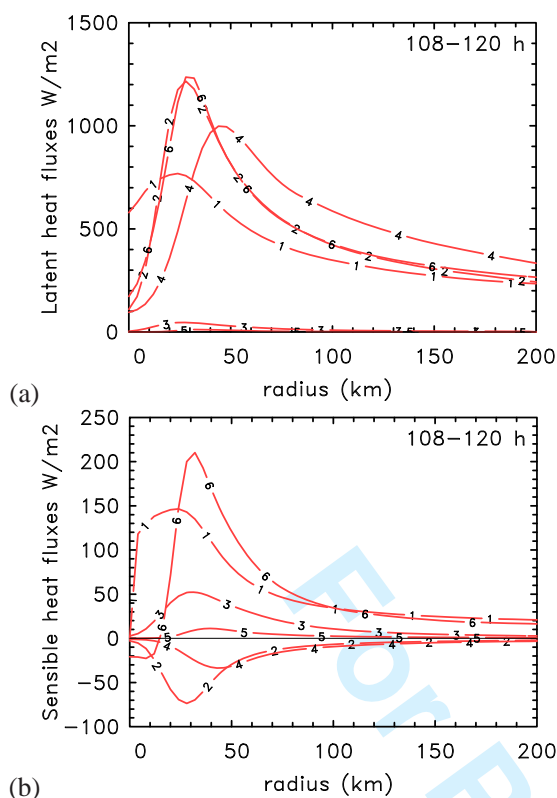


Figure 8. Radial profiles of azimuthal-mean surface (a) latent, and (b) sensible heat fluxes during the period 108-120 hours for the different boundary layer schemes: 1 - modified Bulk scheme, 2 - Blackadar scheme, 3 - Burk-Thompson scheme, 4 - MRF scheme, 5 - Gayno-Seaman scheme, 6 - unmodified Bulk scheme, and 7 - unmodified Gayno-Seaman scheme. Units $W m^{-2}$.

pattern of saturation equivalent potential temperature at any level throughout the free troposphere in the cloudy outflow region and therefore the radial gradient of system buoyancy.

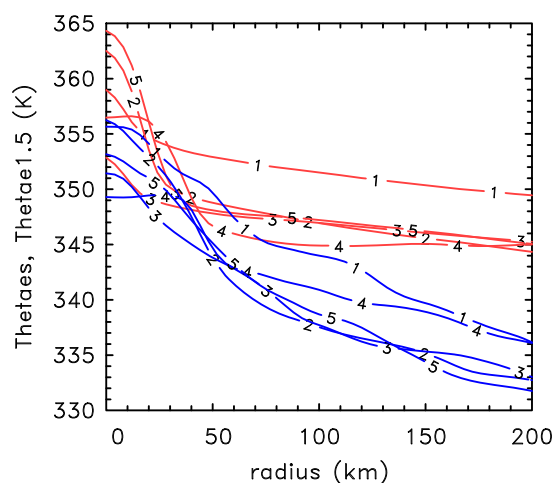


Figure 9. Radial profiles of pseudo-equivalent potential temperature at the surface (red curves) and at a height of 1.5 km (blue curves) at 120 hours in the set of calculations with different boundary layer parameterizations: 1 - modified Bulk scheme, 2 - Blackadar scheme, 3 - Burk-Thompson scheme, 4 - MRF scheme, 5 - Gayno-Seaman scheme, and 6 - unmodified Bulk scheme.

3.10 Eddy diffusivity and TKE

BT00 showed vertical cross-sections of azimuthally-averaged eddy diffusivity for the four schemes that they studied. We performed similar calculations and found similar distributions. We show examples of these in Figure 10 for the Blackadar and MRF schemes, where like other fields, the values are time-averaged over the period 108-120 hours. Both schemes show a low-level maximum of diffusivity in the region of maximum tangential wind speed as well as elevated values in the eyewall updraft (indicated by the $0.2 m s^{-1}$ contour in the figure. Significantly the magnitude of the eddy diffusivity is appreciably larger for the MRF scheme, requiring a different contour interval to be used in the two figure panels. As noted by BT00, the higher diffusivity would account for the relatively large differences in strength between the inflow and upflow in the calculations with the MRF scheme, compared with the others. Maximum values of for the Blackadar scheme are a little less than $90 m^2 s^{-1}$, but fall to values below $30 m^2 s^{-1}$ at radii beyond 100 km. In contrast, maximum values of eddy diffusivity for the MRF scheme exceed $250 m^2 s^{-1}$ and still have values exceeding $50 m^2 s^{-1}$ at radii beyond 200 km. The only observed values that we are aware of are those determined from flight-level wind measurements at an altitude of about 500 m in Hurricane Hugo (1989). These were on the order of $200 m^2 s^{-1}$ beneath the eyewall, where wind speeds were about $60 m s^{-1}$ (Zhang *et al.* 2009). One might be tempted to judge that the MRF scheme is a little too diffusive, whereas the Blackadar scheme is not diffusive enough, but would be inappropriate to draw firm conclusions from a comparison with only one observational estimate!

Retrievals of turbulent kinetic energy (TKE) from Doppler radar data in hurricanes suggest that boundary layer turbulence is being lifted into the eyewall clouds in this region to supplement the turbulence generated locally within the eyewall itself (Lorsolo *et al.* 2009). Thus it is of interest to examine the structure of TKE for the Gayno-Seaman scheme, which is the only scheme to carry this quantity as a prognostic variable. Figure 11 shows a radius-height cross-section of azimuthally-averaged turbulent kinetic energy for this scheme averaged over the period 108-120 hours. The pattern is similar to the patterns of eddy diffusivity shown in Figure 10 with a low-level maximum in the region of maximum tangential wind speed as well as elevated values in the eyewall updraft. As radial gradients of TKE are negative beyond the radius of this maximum, the pattern is suggestive that the local generation of TKE dominates the radial advection thereof. Similar argument cannot be applied to the vertical advection as the vertical gradient of TKE above the TKE maximum is in the direction of the vertical velocity. Nevertheless, TKE values are locally higher in the eyewall updraft, as are the values of diffusivity with the Blackadar and MRF schemes, suggesting that there is an appreciable local generation of TKE in the updraft.

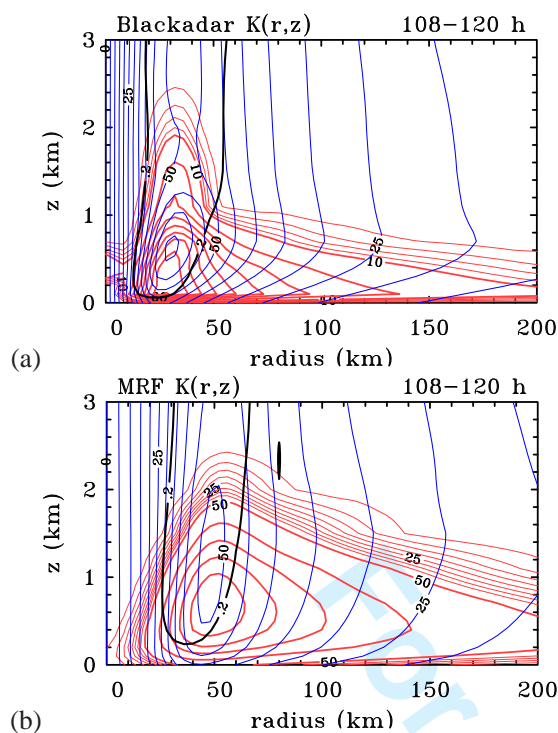


Figure 10. Radius-height cross-section of azimuthally-averaged eddy diffusivity during the period 108-120 hours for: (a) the Blackadar scheme, contour interval $10 \text{ m}^2 \text{ s}^{-1}$, (b) the MRF scheme, contour interval $50 \text{ m}^2 \text{ s}^{-1}$. Thin red contours in (a) show values less than $10 \text{ m}^2 \text{ s}^{-1}$ with an interval of $2 \text{ m}^2 \text{ s}^{-2}$. Thin red contours in (b) show values less than $50 \text{ m}^2 \text{ s}^{-1}$ with an interval of $10 \text{ m}^2 \text{ s}^{-2}$. The thick black contours show the 0.2 m s^{-1} contour of azimuthally-averaged vertical velocity and the thin blue lines show the contours of azimuthally-averaged tangential velocity with a contour interval 5 m s^{-1} .

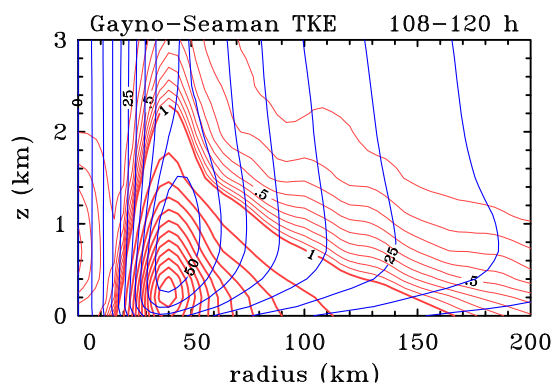


Figure 11. Radius-height cross-section of azimuthally-averaged turbulent kinetic energy during the period 108-120 hours for the Gayno-Seaman scheme. Contour interval $1.0 \text{ m}^2 \text{ s}^{-2}$. Thin contours show values less than $1.0 \text{ m}^2 \text{ s}^{-2}$ with an interval of $0.1 \text{ m}^2 \text{ s}^{-2}$.

4 Conclusions

We have investigated the structure of the boundary layer in an idealized numerical model of a tropical cyclone. The study is motivated by recent findings highlighting the important dynamical role of the boundary layer to tropical-cyclone intensification. The calculations were carried out using the Pennsylvania State University-National Center for Atmospheric Research

fifth-generation Mesoscale Model (MM5). Predictions using one of five of the available schemes were compared, not only between themselves, but where possible with recent observational analyses of boundary layer structure. At this stage the study falls short of being able to advocate the use of a particular scheme, although certain shortcomings of individual schemes are identified in relation to their ability to capture realistic vertical wind profiles and surface inflow angles. The current inability to determine “the optimum scheme” has implications for the predictability of tropical-cyclone intensification.

The paper has drawn further attention to an important problem in the design of deterministic forecast models for hurricane intensity, namely which boundary layer scheme is most appropriate. Clearly a strategy needs to be developed to answer this question. Studies like those of Braun and Tao and Nolan *et al.* discussed earlier are unlikely to be able to determine the “best scheme” by comparing model simulation with observations for the simple reason that other aspects of the model such as the representation of cloud microphysics have inherent uncertainties as well. In this regard, diagnostic studies of the type described by Kepert and coworkers might be more suited to providing an answer to the foregoing problem, subject to the caveats discussed by Smith and Montgomery (2009), but they should be extended to consider different schemes. What our study and that of Braun and Tao can provide is an estimate of forecast uncertainty that is coupled with the uncertainty in knowing the optimum boundary layer scheme to use.

5 Appendix: The boundary-layer schemes

5.1 The bulk scheme

The Bulk scheme calculates the fluxes of sensible heat, latent heat and momentum at the ground by a bulk-aerodynamic parameterization. The fluxes between the individual model layers within the boundary layer are then calculated by a first-order (local K -mixing) scheme. The original parameterization calculates the Bulk-Richardson number to distinguish between a stable and an unstable case. The surface drag and heat and moisture exchange coefficients are the only variables that are then calculated dependingly on the stability of the boundary layer. After the changes we made there is no distinction between a stable or unstable boundary layer in the bulk scheme. In the unmodified version of the scheme, the exchange coefficients are given by $C_u = [C_{uN}^{-1} - 25 \exp(0.26\zeta - 0.030\zeta^{-2})]^{-2}$, $C_E = (C_{\theta N}^{-1} + C_u^{-1} - C_{uN}^{-1})^{-1}$, in the *unstable case* ($Ri_B < 0$), where $\zeta = \log_{10}(-Ri_B) - 3.5$, and $C_u = C_{uN}(1 - Ri_B/Ri_c)$, $C_\theta = C_{\theta N}(1 - Ri_B/Ri_c)$, in the *stable case* ($0 \leq Ri_B \leq 0.9Ri_c$). In both cases, $C_{uN} = [k^{-1} \log\{0.025(\bar{h} - \bar{z}_s)/z_0\} + 8.4]z^{-1}$, $C_{\theta N} = (k^{-1}R \log\{0.025(\bar{h} - \bar{z}_s)/z_0\} + 7.3)^{-1}$, with the critical bulk Richardson number given by $Ri_c = 3.05$. The constant $k = 0.35$ is the Kármán constant, the constant $R = 0.74$ is used in the surface-layer temperature profile function, z_0 is the roughness length, \bar{h} is a

horizontal average of the planetary boundary-layer height above mean sea level, \bar{z}_s is a horizontal average of the surface height above mean sea level and Ri_B is the bulk Richardson number.

5.2 The Blackadar scheme

The Blackadar scheme (Blackadar 1976) was first introduced as a representation of the nocturnal boundary layer. The version used here was extended by Blackadar (1978, 1979) and Zhang and Anthes (1982) to account also for the daytime boundary layer. The present scheme has two modules: one for the day-time convective state and one for the night-time stable states. The module that is invoked depends on the vertical temperature gradient in the lowest model layer and on the magnitude of $|z_h/L|$, where z_h is the height of the mixed layer and L is the Monin-Obukhov length. The vertical temperature gradient in the lowest model layer is characterized by the bulk Richardson number Ri_b . In the nocturnal module, the atmosphere is assumed to be stably stratified, or at most slightly unstable, and a first-order closure scheme is used. To account for the largest gradients, which generally occur in the lowest layer, a surface layer of 10 m depth is used, based on Monin-Obukhov similarity theory. The module for the nocturnal boundary layer is subdivided into three stability states. The night-time stable state is assumed when $Ri_b \geq 0.2$, the damped mechanical turbulent state when $0 < Ri_b < 0.2$ and the forced convection state when $Ri_b \leq 0$ and $|z_h/L| \leq 1.5$. The daytime module allows for free convection and is active when $Ri_b \leq 0$ and $|z_h/L| \geq 1.5$. Discrete matrix forms of nonlocal theory are then used to parameterize convective circulations. In nonlocal theory, the vertical transfer of momentum, heat and moisture is not determined by the local mean gradient, but by the thermal structure of the whole mixed layer. The Blackadar scheme is the only one of those studied that applies transilient mixing in any of the stability states, i.e., which allows mixing between non-adjacent vertical layers.

5.3 The Mellor-Yamada-based schemes

Both Mellor-Yamada-based schemes described here use a one-and-a-half-order closure, which refers to level-2.5 in the Mellor-Yamada hierarchy (Mellor and Yamada 1974). A comprehensive summary of the different closures is given by Stull (1988). In a one-and-a-half-order closure the eddy exchange coefficient of an adiabatically conserved quantity is related to the predicted TKE. This kind of scheme is often referred to as a ‘‘TKE scheme’’.

5.3.1 The Burk-Thompson scheme

The Burk-Thompson scheme was originally designed for the marine boundary layer (Burk and Thompson, 1982) and incorporated both level 2.5 and 3.0 schemes. The early versions of the scheme, which were implemented in the US-Navy’s Navy Operational Regional Atmospheric Prediction System (NORAPS), apply a higher vertical

resolution than that in the model and include a counter-gradient flux term for temperature. These two features are not implemented in MM5 and only the level 2.5 version is available. The Louis (1979) scheme is used to parameterize the surface layer and applies an empirical fit to the Businger profile functions. Neither horizontal advection, diffusion, or vertical advection of TKE are included in this scheme.

5.3.2 The Gayno-Seaman scheme

The Gayno-Seaman scheme is a level-2.5 Mellor-Yamada-based scheme. In order to represent cloud water in a consistent way, the model uses liquid water potential temperature, θ_L , and total water mixing ratio, q_T , which are both conserved thermodynamic variables in non-precipitating clouds (Betts, 1973). The turbulent vertical transport of θ_L is parameterized using a counter-gradient heat flux term, based on the sensible heat flux, boundary layer height, and the convective vertical velocity scale (Therry and Lacarriere, 1983). The Gayno-Seaman scheme is the only one in MM5 for which TKE is treated as a prognostic quantity and for which TKE is advected. The surface fluxes for the Gayno-Seaman scheme are based on the same Monin-Obukhov similarity parameterization used with the Blackadar scheme and the stability states are determined using the same criteria (Shafran, 2000). In the unmodified version of the scheme, the momentum exchange coefficient is given by $C_u = k(\theta_e - \theta)/(GZ10Z0 - \psi_H)$, where $GZ10Z0 = \log(\max(z, 10)/z_0)$, and z_0 is the roughness length. The enthalpy exchange coefficient, C_E is zero under night time stable conditions and conditions of damped mechanical turbulence and has the value $-Ri_B h/z$ under conditions of forced convection and $-h/L$ under conditions of free convection. Here L is the Monin-Obukhov length, z is the height above surface, h is the height above surface of the planetary boundary layer, Ri_B is the bulk Richardson number, θ is the potential temperature, θ_e is the pseudo-equivalent potential temperature ψ_H is a similarity function and again k is the Kármán constant.

5.4 The MRF scheme

The MRF scheme was developed initially for the United States National Centers for Environmental Prediction (NCEP) Medium Range Forecast system by Hong and Pan (1996) and was implemented in MM5 by Dudhia and Hong, as stated in the corresponding piece of code. This scheme applies nonlocal K -mixing for potential temperature and water vapour mixing ratio in the mixed layer, moist vertical diffusion in clouds, and local K -mixing above clouds. The nonlocal mixing is implemented following a nonlocal diffusion concept by Troen and Mahrt (1986). The term ‘‘nonlocal’’ as it appears in the literature is a little misleading. It refers here to the flux of a particular quantity between adjacent layers calculated by applying a correction term for the local gradient. This

correction term incorporates the contribution of the large-scale eddies to the total flux, thus allowing for counter-gradient fluxes. The eddy exchange coefficients, K , are calculated from a prescribed profile function of boundary layer heights and scale parameters. The surface fluxes are calculated in the same way as in the Blackadar scheme.

The four boundary-layer stability states are determined using only the bulk Richardson number: In the night-time stable state ($Ri_b \geq 0.2$), all scaling parameters at the surface and all turbulent fluxes are set equal to zero. In the nocturnal damped mechanical turbulent state ($0 < Ri_b < 0.2$), the scaling parameters are determined by Ri_b and L (the Monin-Obukhov length). In the nocturnal, forced-convection state ($Ri_b = 0$), the scaling parameters are determined by the local Richardson number Ri only (local K -theory). When $Ri_b < 0$, the daytime module is used and the counter-gradient terms take effect.

6 Acknowledgements

This research was supported by a grant from the German Research Council (Deutsche Forschungsgemeinschaft). We have benefited from many discussions about the boundary layer with Michael Montgomery. We are most grateful to Saurabh Barve and Sang Nguyen for their help in tracking down a subtle coding error in the Bulk scheme in MM5.

References

- Anthes RA Chang SW. 1978 Response of the hurricane boundary layer to changes of sea-surface temperature in a numerical model. *J. Atmos. Sci.*, **35**, 1240-1255
- Bell MM and Montgomery MT. 2008 Observed structure, evolution, and potential intensity of Category 5 Hurricane Isabel (2003) from 12 to 14 September. *Mon. Wea. Rev.*, **65**, 2025-2046
- Betts AK. 1973 Non-precipitating cumulus convection and its parameterization. *Q. J. R. Meteorol. Soc.*, **99**, 178-196
- Black PG D'Asoro EA Drennan WM French JR Niller PP Sanford TB Terril EJ Walsh EJ Zhang JA 2007 Air-sea exchange in hurricanes. Synthesis of observations from the coupled boundary layer air-sea transfer experiment. *Bull. Amer. Meteorol. Soc.*, **88**, 357-374
- Blackadar AK. 1976 Modelling the nocturnal boundary layer. Third Symp. on Atmospheric Turbulence, Diffusion and Air Quality. Raleigh, Amer. Meteor. Soc. 46-49
- Blackadar AK. 1978 Modelling pollutant transfer during daytime convection. Fourth Symp. on Atmospheric Turbulence, Diffusion and Air Quality, Reno, Amer. Meteor. Soc. 443-447
- Blackadar AK. 1979 High resolution models of the planetary boundary layer. *Advances in Environmental Science and Engineering*. 50-52
- Braun, SA Tao W-K. 2000 Sensitivity of high-resolution simulations of Hurricane Bob (1991) to planetary boundary layer parameterizations. *Mon. Wea. Rev.*, **128**, 3941-3961
- Bui HB Smith RK Montgomery MT Peng J. 2009 Balanced and unbalanced aspects of tropical-cyclone intensification. *Q. J. R. Meteorol. Soc.*, **135**, 1715-1731
- Burk SD Thompson WT. 1982 Operational Evolution of a Turbulence Closure Model Forecast System. *Mon. Wea. Rev.*, **110**, 1535-1543
- Dudhia J. 1993 A non-hydrostatic version of the Penn State-NCAR mesoscale model: Validation tests and simulation of an Atlantic cyclone and cold front. *Mon. Wea. Rev.*, **121**, 1493-1513
- Franklin JL Black ML Valde K. 2003 GPS dropwindsonde wind profiles in hurricanes and their operational implications. *Wea. Forecasting*, **18**, 32-44
- Grell GA Dudhia J and Stauffer DR. 1995 A description of the fifth generation Penn State/NCAR mesoscale model (MM5). NCAR Tech Note NCAR/TN-398+STR, 138 pp.
- Hong S-Y Pan H-L. 1996 Nonlocal boundary layer vertical diffusion in a medium-range forecast model. *Mon. Wea. Rev.*, **124**, 2322-2339.
- Janjić ZI. 1990 The step-mountain coordinate: Physical package. *Mon. Wea. Rev.*, **118**, 1429-1443
- Janjić ZI. 1994 The step-mountain eta coordinate model: Further developments of convection, viscous sub-layer, and turbulence closure schemes. *Mon. Wea. Rev.*, **122**, 927-945
- Jordan CL. 1958 Mean soundings for the West Indies area. *J. Meteor.*, **15**, 91-97
- Keperth JD. 2001 The dynamics of boundary layer jets within the tropical cyclone core. Part I: Linear Theory. *J. Atmos. Sci.*, **58**, 2469-2484
- Keperth JD Wang Y. 2001 The dynamics of boundary layer jets within the tropical cyclone core. Part II: Nonlinear enhancement. *J. Atmos. Sci.*, **58**, 2485-2501
- Keperth JD. 2006a Observed boundary-layer wind structure and balance in the hurricane core. Part I. Hurricane Georges. *J. Atmos. Sci.*, **63**, 2169-2193
- Keperth JD. 2006b Observed boundary-layer wind structure and balance in the hurricane core. Part II. Hurricane Mitch. *J. Atmos. Sci.*, **63**, 2194-2211
- Lorsolo S Zhang JA Marks F Gamache J. 2009 Estimation and mapping of hurricane turbulent energy using airborne Doppler measurements. Submitted to *Mon. Wea. Rev.*,
- Louis JF. 1979 A parametric model of vertical eddy fluxes in the atmosphere. *Bound. Layer Met.*, **17**, 187-202

- 1
2
3 Mellor GL Yamada T. 1974 A Hierarchy of Turbulence
4 Closure Models for Planetary Boundary Layers. *J.*
5 *Atmos. Sci.*, **31**, 1791-1806
- 6 Montgomery MT Nicholls ME Cram TA and Saunders
7 AB. 2006a A vortical hot tower route to tropical
8 cyclogenesis. *J. Atmos. Sci.*, **63**, 355-386
- 9 Montgomery MT Bell MM Aberson SD and Black ML.
10 2006b Hurricane Isabel (2003): New insights into
11 the physics of intense storms. Part I Mean vortex
12 structure and maximum intensity estimates. *Bull.*
13 *Amer. Meteorol. Soc.*, **87**, 1335 - 1348
- 14 Montgomery MT Nguyen SV and Smith RK. 2008 Do
15 tropical cyclones intensify by WISHE?. *Q. J. R.*
16 *Meteorol. Soc.*, **135**, 1697-1714
- 17 Nguyen CM Smith RK Zhu H and Ulrich W. 2002 A
18 minimal axisymmetric hurricane model. *Q. J. R.*
19 *Meteorol. Soc.*, **128**, 2641-2661
- 20 Nguyen SV Smith RK and Montgomery MT. (M1) 2008
21 Tropical-cyclone intensification and predictability
22 in three dimensions. *Q. J. R. Meteorol. Soc.*, **134**,
23 563-582
- 24 Nolan DS Zhang JA Stern DP. 2009a Evaluation of plan-
25 etary boundary layer parameterizations in tropi-
26 cal cyclones by comparison of in-situ observations
27 and high-resolution simulations of Hurricane Isabel
28 (2003). Part I: Initialization, maximum winds, and
29 the outer core boundary layer. *Mon. Wea. Rev.*, **137**,
30 in press
- 31 Nolan DS Zhang JA Stern DP. 2009b Evaluation of plan-
32 etary boundary layer parameterizations in tropi-
33 cal cyclones by comparison of in-situ observations
34 and high-resolution simulations of Hurricane Isabel
35 (2003). Part II: Inner core boundary layer and eye-
36 wall structure. *Mon. Wea. Rev.*, **137**, in press
- 37 Powell MD Uhlhorn EW Kepert JD. 2009 Estimating
38 maximum surface winds from hurricane reconnais-
39 sance measurements. *Wea. Forecasting*, **24**, 868-883
- 40 Schwendike J Kepert JD. 2008 The boundary layer winds
41 in Hurricane Danielle 1998 and Hurricane Isabel
42 2003. *Mon. Wea. Rev.*, **136**, 3168-3192
- 43 Shafran PC Seaman NL Gayno GA. 2000 Evaluation of
44 Numerical Predictions of Boundary Layer Structure
45 during the Lake Michigan Ozone Study. *J. Appl.*
46 *Met.*, **39**, 412-426
- 47 Smith RK. 2003 A simple model of the hurricane bound-
48 ary layer. *Q. J. R. Meteorol. Soc.*, **129**, 1007-1027
- 49 Smith RK. 2006 Accurate determination of a balanced
50 axisymmetric vortex. *Tellus*, **58A**, 98-103
- 51 Smith RK Vogl S. 2008 A simple model of the hurricane
52 boundary layer revisited. *Q. J. R. Meteorol. Soc.*,
53 **134**, 337-351
- 54 Smith RK Montgomery MT. 2009 Hurricane boundary-
55 layer theory. Submitted to *Q. J. R. Meteorol. Soc.*,
- 56 Smith RK Montgomery MT Zhu H. 2005 Buoyancy in
57 tropical cyclone and other rapidly rotating atmos-
58 pheric vortices. *Dyn. Ocean Atmos.*, **40**, 189-208
- 59
60 Smith RK Montgomery MT Nguyen SV. (M3) 2009 Tropi-
cal cyclone spin-up revisited. *Q. J. R. Meteorol.*
Soc., **135**, 1321-1335
- Stull, RB. 1988 An introduction to boundary layer meteor-
ology. Kluwer, Dordrecht, Holland, pp680
- Therry G Lacarrere P. 1983 Improving the eddy kinetic
energy model for planetary boundary layer descrip-
tion. *Bound. Layer Met.*, **25**, 63-88
- Troen IB Mahrt L. 1986 A simple model of the atmos-
pheric boundary layer; sensitivity to surface evapo-
ration. *Bound. Layer Met.*, **37**, 129-148.
- Zhang D-L Anthes RA. 1982 A High-Resolution Model
of the Planetary Boundary Layer - Sensitivity Tests
and Comparisons with SESAME-79 Data. *J. Appl.*
Met., **21**, 1594-1609
- Zhang D-L Liu Y Yau MK. 2001 A multi-scale numerical
study of Hurricane Andrew (1992). Part IV: Unbal-
anced flows. *Mon. Wea. Rev.*, **129**, 92-107